Surface-Controlled Water Flow in Nanotube Membranes

Surface-controlled water flow in nanotube membranes

Serena Casanova†, Matthew K. Borg‡, Y.M. John Chew†, Davide Mattia†*

† Department of Chemical Engineering and Centre for Advanced Separations Engineering, University of Bath, Bath, BA2 7AY, UK
‡ School of Engineering, University of Edinburgh, Edinburgh, EH9 3FB, UK
* Address correspondence to d.mattia@bath.ac.uk

Abstract

The independent effect of nanotube surface chemistry and structure on the flow of water under nanoscale confinement is demonstrated in this paper for the first time via the synthesis of novel carbon nitride nanotube (CNNT) membranes. Using a combination of experiments and high-fidelity molecular dynamics (MD) simulations, it is here shown that the hydrophilisation of the sp^2 carbon structure, induced by the presence of the C-N bonds, decreases the pure water permeance in CNNTs when compared with pristine and turbostratic carbon nanotubes (CNTs). The MD simulations are based on a model true to the chemical structure of the synthesized nanotubes, and built from material spectroscopy measurements and calibrated potentials using droplet experiments. The effect on permeance is explained in terms of solid-liquid interactions at the nanotube wall with increased water viscosity and decreased surface diffusion near the CNNT wall, when compared to CNTs. A model directly linking the solid-liquid interactions to the water permeance is presented, showing good agreement with both experiments and MD simulations. This work opens the way to tailoring surface chemistry and structure inside nanotube membranes for a wide range of transport and separation processes.

Keywords: Carbon nitride nanotubes; Permeance; Anodic alumina membrane; Chemical vapour deposition; Ultrafiltration; Molecular Dynamics

The high water flow enhancement observed in carbon nanotubes (CNTs)[1] has, over the years, been attributed to a variety of causes,[2-3] from confinement effects at the nanoscale to the nature of the physical and chemical interactions between the liquid and the tubes' wall, to more questionable explanations such as air gaps or depletion layers at the interface between the two. As nanotubes, and now 2D materials, are incorporated in mixed matrix membranes or fabricated as stand-alone membranes, elucidating the origin of the flow enhancement phenomenon remains crucial to tailor the materials for specific applications, ranging from seawater desalination[4] to removal of pollutants in nanofiltration.[5]

The effect of confinement has been well-researched and is now well understood, including a threshold below which continuum fluid mechanics no longer applies,[6] the presence of slip, i.e. low resistance to liquid flow,[7] and how both are affected by the curvature of the tube.[8]

The picture regarding the effect of physico-chemical interactions on flow is less clear: While flow enhancement is generally attributed to the 'hydrophobic nature' of carbon, the contact angle of water on pristine graphite surfaces is just below 90 degrees,[3] a key aspect explaining why water naturally imbibes into CNTs.[9-10] Furthermore, water flow enhancement has been shown to occur – to varying degrees – in materials much more 'hydrophilic' than carbon (i.e. with lower water contact angle),[11] for example silicon carbide.[12] While the above results have been obtained via molecular dynamics (MD) alone, modest flow enhancement has also been observed experimentally in silica,[13] and alumina[14] nanochannels and in turbostratic carbon nanotube membranes.[15] To further complicate the picture, recent experiments showed little to no water flow enhancement in boron nitride tubes (BNNTs),[8] a material that has a very similar water contact angle to graphite,[16] while MD simulations of water flow in BNNTs showed significant enhancement, though still less than CNTs.[17] It has long been hypothesised, via simulations, that hydrophilic nanochannels or nanotubes, with either larger surface-liquid energy,[18] or/and surface polarity,[19] have the effect of decreasing flow, resulting in small[20] or zero hydrodynamic slip length.[21] MD studies imposing more hydrophilic potentials (e.g. that of silicon) on the sp^2 carbon structure showed a drastic decrease of the water flow rate.[22] Furthermore, MD simulations have also shown that creating defects in the carbon structure (i.e. missing carbon atoms) leads to a decrease in flow rates,[23] as did the addition of functional groups on the wall's surface.[24-25] In all these instances, however, it is difficult to separate the effect on flow arising from changes in the structure (e.g. defects, roughness) from those occurring in the surface chemistry (e.g. presence of functional groups) of the nanotube wall materials.

Several theoretical models have been developed to explain these effects,[7, 19] with most focusing on the slip length, L_s, as defined in the Hagen-Poiseuille equation with Navier slip at the nanotube walls:

$$q = \frac{\pi D^4 \Delta P}{128\,\mu L}\left(1 + \frac{8L_s}{D}\right), \tag{1}$$

where ΔP is the applied pressure, μ is the fluid viscosity, and q is the volume flow rate through one nanotube of diameter D and length L. It should be noted that while the above equation is strictly valid only for continuum transport (i.e. when no confinement occurs) it has also been used to provide insight into non-continuum transport phenomena.[26-27] The ratio of Eq. (1) to the no-slip case yields the flow enhancement:

$$\varepsilon = 1 + \frac{8L_s}{D}. \tag{2}$$

Equation (1) can be transposed to a membrane (i.e. a structure containing a large number of aligned nanotubes) if the tubes' size distribution and membrane porosity are known.[15] Under the assumption that all n nanotubes in the membrane have a narrow size distribution, one obtains the following expression for the permeance, K, which is of relevance to membrane scientists:

$$K = \frac{Q}{\Delta P\ A_{mem}} = \frac{\phi D^2}{32\ \mu L}\left(1 + \frac{8L_s}{D}\right), \quad (3)$$

where A_{mem} is the membrane's area, ϕ is the porosity and $Q = q\ n$ is the total flow rate through the membrane.

In this manuscript, the effect on water flow enhancement caused by modifying the surface chemistry and structure of carbon nanotubes *independently*, is demonstrated through a combination of experiments and MD. This has been achieved by fabricating novel carbon nitride nanotube (CNNT) membranes. Carbon nitride nanotubes have a similar surface structure to carbon nanotubes but with the presence of C-N bonds, which significantly change their surface chemistry,[28] without significantly altering their structure (i.e. sp^2 network).[29] The CNNT membranes have been prepared via chemical vapour deposition inside anodic alumina membranes, modifying a previously developed pyrolisation process.[30] This approach does not use the toxic reagents previously employed[28] and, more relevant to this work, produces CNNTs with lower carbon to nitrogen ratios.[31] This allows a direct comparison with published experimental data for carbon nanotube membranes produced inside anodic alumina membranes (AAMs).[15]

The experimental and MD results presented in this work show that changes to the carbon nanotubes' structure (i.e. transition from graphitic to turbostratic) and surface chemistry (i.e. carbon to carbon nitride) affect water flow enhancement. The approach proposed here allows decoupling these two effects, opening new ways to tailoring the nanotubes' surface chemistry and structure for specific applications.

Results and Discussion

This work aims at testing the flow of pure water in carbon nitride nanotubes and, in conjunction with MD, assess the extent of the effect of differences in surface chemistry and structure on flow enhancement, when compared to carbon nanotubes.

CNNT Membrane Synthesis: After synthesis, CNNT membranes appear yellow in colour (Figure S 1). The surface is clean with open pores (Figure 1a), ranging from 11.4 ± 2.1 nm to 76.1 ± 4.7 nm in diameter, depending on the starting AAM used and synthesis conditions. When the AAM is partially dissolved in H_3PO_4, the CNNTs stick out from the pores, showing they are indeed hollow (Figure 1b). This can be observed in greater detail in the uncropped FESEM micrograph in the Supplementary Information (Figure S 2a).

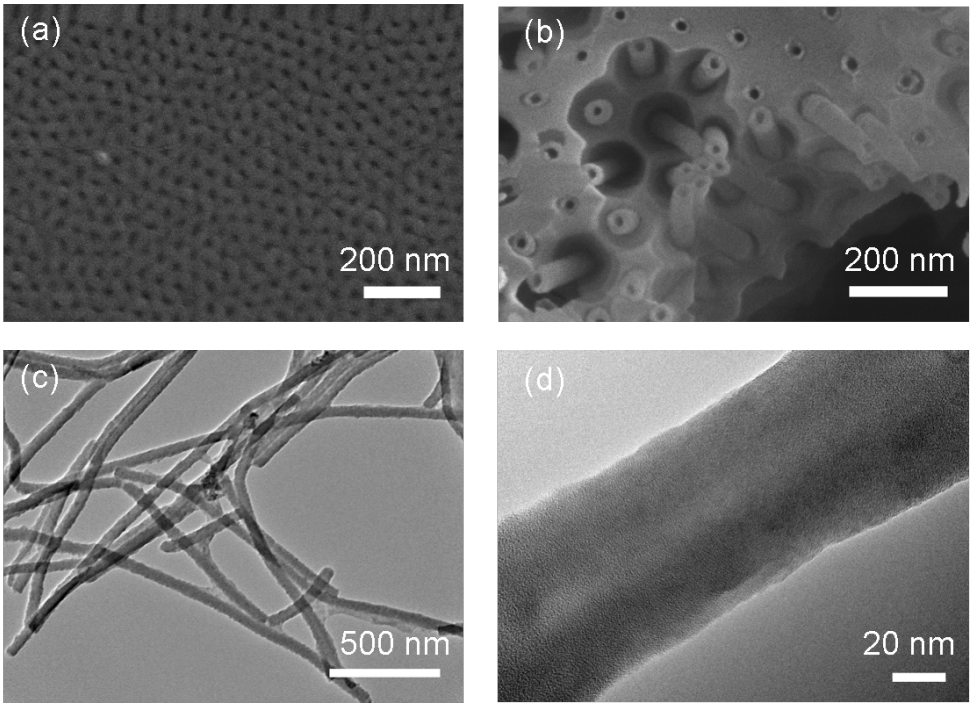

Figure 1. FESEM micrographs of (a) a CNNT membrane surface and (b) CNNTs protruding from an AAM partially dissolved in H_3PO_4 for 45 minutes; TEM micrographs of (c) CNNTs released from the AAM template, and (d) showing their hollow structure.

TEM micrographs of CNNTs released from the AAM (Figure 1c and Figure S 2b), also confirm tubular features (Figure S 2b) with a turbostratic structure (Figure S 2d), similar to that of CNT membranes produced using the same CVD process.[15] This change in the surface chemistry with the introduction of N implies a variation in atomic structure and bonding, but not in the supramolecular turbostratic structure of the nanotubes. The CNNTs have outer tube diameters comparable to the size of the membrane pores. For the membrane shown in Figure S 2b, statistical image analysis using ImageJ showed an average AAM pore size of 37.6 ± 3.2 nm, while the average tube outer diameter size is 37.3 ± 5.1 nm. It is observed that a side-effect of the process employed to release the CNNTs from the AAM templates is that the resulting tubes are partially covered by the by-products of the dissolution process (Figure 1c). These side-effects are not present in those membranes used for flow testing as they were not subjected to this procedure. While the external walls of the deposited CNNTs had a high degree of roughness, caused by the patterning from the alumina template surface, the inner surface of the analysed tubes was smooth and lacked this same pronounced roughness (Figure S 2c).

X-ray photoelectron spectroscopy (XPS) analysis of CNNTs reveals a C:N atomic ratio of 1.47 and allows identifying the percentage of pyridinic and quaternary nitrogen based on their binding energies at 398.9 eV and 400.6 eV respectively,[32-33] as shown in Figure 2a. The structure of the CNNTs was compared to that of turbostratic CNTs prepared via a similar non-catalytic CVD process inside the pores of AAMs (Figure S 3).[15] A well-established method was used to quantify the C=C sp^2 bonding in the carbon structure and that of different functional groups (i.e. COH, C-O-C, C=O) and vacancies:[34] This method allowed quantifying the percentage of defects, relating it to the broadening of the C1s line shape in the XPS spectra. For CNTs,

carbon in the graphitic sp^2 form was found to account for 91.2 atomic % of the sample, while defects accounted for the remaining 8.6% ± 0.6%. CNNTs had a comparable amount of carbon defects that accounted for the 11.6% ± 1.3%. High resolution XPS spectra of C1s for CNNTs and CNTs with peaks identification can be found in Figure S 4.

Figure 2b compares the Raman spectra of CNNTs membranes in this work and turbostratic CNTs membranes previously synthesized,[15] showing the characteristic D- and G-bands. For the CNNT spectra, additional Raman bands at 700 cm^{-1} and 900 cm^{-1} are identified as the N-breathing and bending vibrations of heterocyclic molecules containing the triazine ring species.[35] Bands between 1200 cm^{-1} and 1700 cm^{-1} are attributed to the G- and D-band with disordered graphitic carbon and observable also in carbon-nitride materials.[36]

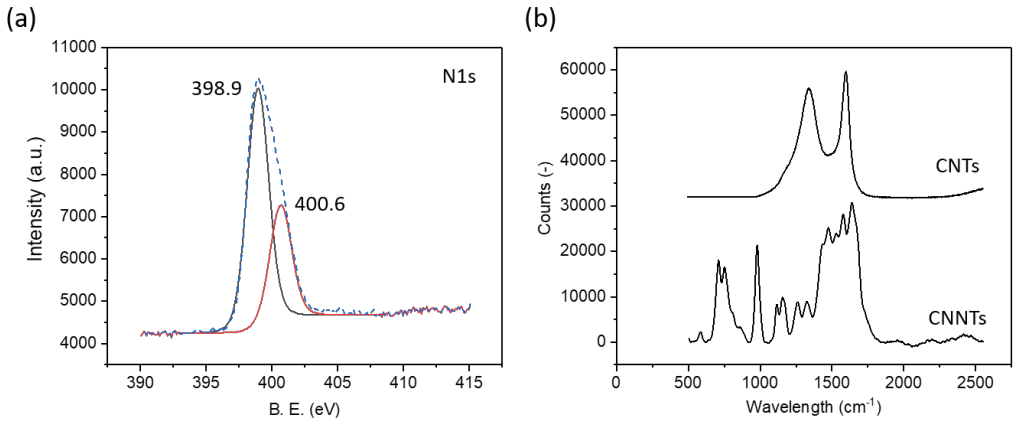

Figure 2. (a) High-resolution XPS spectra of the N1s region showing the graphitic species (black line) and the pyridinic species (red line); (b) Raman spectra for CNNTs and CNTs.

Molecular surface model of CNTs and CNNTs: The XPS data was used to build the CNT and CNNTs used in the MD simulations. An example of the MD surface for a (60,60) CNNT with diameter D = 8.14 nm is shown in Figure 3a. The amount of carbon and nitrogen atoms of the nanotube is 60% and 40%, respectively, with pyridinic (~13%) and quaternary (~27%) microscopic structures, obtained from the XPS results, randomly distributed on the surface of the tubes. Figure 3b shows the point charge distribution on a small section of a CNNT surface. Using charge-equilibration calculations on these CNNT configurations, it was found that the nitrogen atoms are negatively charged (-0.4 e to -0.7 e), while the carbon atoms are positively charged when surrounded by nitrogen atoms or with zero charge in carbon-only areas. More information about constructing the CNNTs and obtaining point charges, including the MD methodology, can be found in the Methods section.

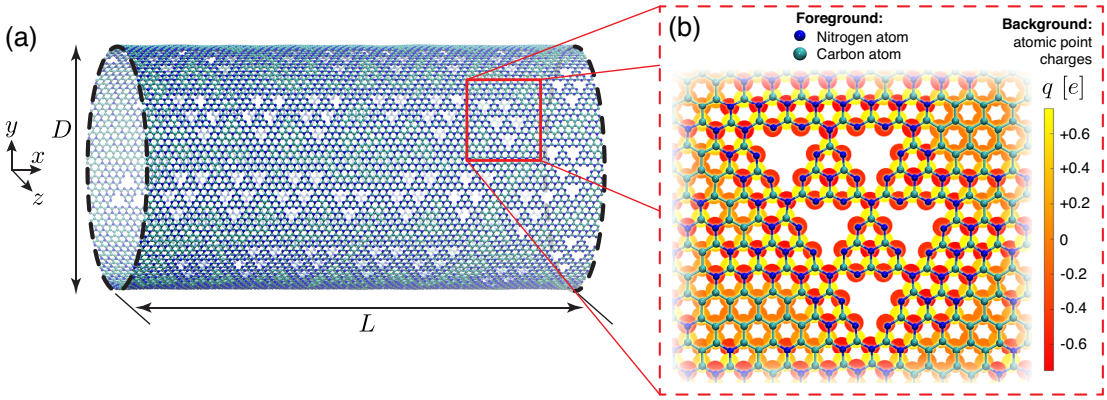

Figure 3. (a) Molecular dynamics setup of a CNNT (showing only the inner tube of a double-wall CNNT) of diameter D = 8.14 nm, chirality (60,60), and length L=15.74 nm (blue atoms are nitrogen, and cyan atoms are carbon); (b) point charges on a representative small sample of the CNNT surface.

Wettability Measurements: Literature reports contact angles values for turbostratic CNTs produced by CVD in the range between 61º and 90º,[15] whereas the contact angles for highly graphitic CNTs have been found to be 82 - 86º.[37] The contact angle of the CNNTs in this work was measured to be in the range 43 - 67º, after being adjusted for roughness with the Wenzel equation, with an average of 53º. This is in agreement with results for flat films in the literature.[36] These values are reported in Table 1.

Permeance in CNNT Membranes: Experimental results of pure water permeance through CNNTs with inner diameter ranging from 11.4 ± 2.1 nm to 76.1 ± 4.7 nm show an expected quadratic dependence of water permeance on pore diameter (reported as permeance K, with units LMH @ 1 bar in Table S 1). Here though, results are presented as $[KL\mu/\phi]^{0.5}$ vs. D to enable comparing results between different materials and sets of experiments. Each experimental data point is the average of 2 to 6 measurements on the same membrane for different transmembrane pressures. All the data collected for the study are reported in Figure 4. The scatter in the experimental data can be associated to non-evident partial cracks, imperfections in the starting templates or potential pore clogging.

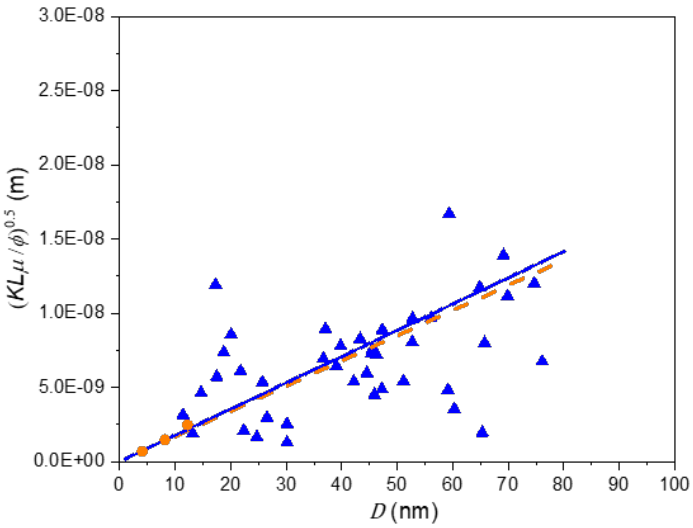

Figure 4. Comparison of permeance measurements between experiments (▲) and molecular dynamics simulations (●). The MD results are obtained by measuring flow rate in three CNNTs of different diameters. The dashed orange line (-) extrapolates the measurements of flow resistance R from these MD simulations using only the assumption that flow rate $q \sim D^4$, as expected in Eq.(1), while the straight blue line (-) uses directly Eq. (3) for flow rate derived from the H-P relationship, with slip length calculated from MD. Data are plotted as the square root of $KL\mu/\phi$ (m) versus pore diameter D (nm).

All MD simulations in this work have been constructed to be as close as possible to experimental conditions, including having the same surface structure and surface chemistry as those measured from the experiments, as well as using a realistic water model that models accurately the condensed phase of water (see Methods section). All results from these MD simulations are provided in the Supplementary Information.

MD simulations of water flow through CNNTs show good agreement with the experimental data. The orange circle symbols in Figure 4 are MD simulations of water transport through different CNNT diameters (4 nm, 8 nm, 12 nm). Note that the scope of using the term $KL\mu/\phi$ on the y-axis of Figure 4 is also to normalise permeance with membrane geometry, thereby allowing MD simulations in single nanotubes to be compared directly with membrane experiments. Furthermore, as the experimental membranes have much larger CNNT diameters D than what can be tractably simulated using MD, the solid and dashed lines in Figure 4 indicate theoretical predictions using input from the MD flow measurements. The solid blue line uses Eq.(3) with slip length (L_s < 1 nm) computed from the MD, while the dashed orange line assumes that the flow rate has a relationship that depends on D^4, as per Eq.1. It is important to highlight that the MD data and predictions are independent of permeance or membrane parameters (such as length or porosity) measured in the experiments; i.e. solid and dashed lines in Figure 4 are not fits of the experimental data points. MD simulations also confirmed that nanotube end losses are negligible for these membrane thicknesses, and so do not need to be incorporated in Eq.(3).[38]

The comparison between experimental and the independent MD predictions (solid blue line) shows coefficients of correlation of 0.63. This indicates a strong

relationship between MD results and experimental data, while *p*-values lower than 0.05 (1×10^{-5} for CNNTs) indicate a very significant prediction, where changes in the predictor's value are strongly related to changes in the response value.[39] This serves as further validation of the usefulness of this MD model for the description of flow in nanosized channels. The same process was repeated for the turbostratic CNT membranes previously published,[15] with correlation of 0.88 between MD and experimental data and *p*-value of 2×10^{-22} (Figure S 6). The very good correlation between experimental and MD data, allows to go a step further and compare the permeance of graphitic and turbostratic CNTs with CNNTs (Figure 5). As experimental data for graphitic CNT membranes (i.e. pristine rolled graphene sheets) are rare, especially for these large diameters, in Figure 5 predictions using Eq. (3) are plotted, with slip length derived from MD simulations of flow through CNTs.

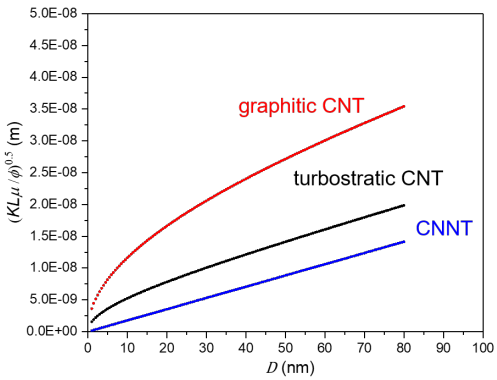

Figure 5. Comparison of permeance, Eq.(3), using slip lengths derived from MD simulations (see Table 1) plotted as the square root of $KL\mu/\phi$ (m) versus pore diameter D (nm).

The comparison clearly shows a decrease in water permeance from the graphitic to the turbostratic CNTs and a further decrease for water permeating through CNNTs with the same diameter. The reduction in permeance between graphitic and turbostratic CNTs is attributed to a change in the sp^2 surface structure of the carbon nanotubes,[22-23] i.e. a decrease in graphitization, already measured in the turbostratic tubes[37] and higher surface wettability. In order to match this less organised structure, the CNT used in the present MD simulations had a degree of defects set to match the XPS results and surface/liquid potentials calibrated from sessile droplet experiments.

On the other hand, the transition in Figure 5 from turbostratic CNT to CNNT, is attributed primarily to a change in the surface chemistry due to the hydrophilising effect on the sp^2 carbon structure induced by the C-N bond. This is the first experimental observation of what postulated by previous MD work where a dependence of water permeance on an artificially imposed degree of hydrophobicity of the CNT structure was observed.[18, 40]

The MD simulations also show that the presence of the C-N bonds dramatically changes the surface/liquid interfacial energy landscape of the CNNTs, compared to a pristine CNT. Inspecting the water ordering near the CNNTs from the radial density distribution measurements of water, reveals that the triazine rings act as local 'potential energy wells' (Figure 6a for oxygen atoms). These wells - indicated by the small blue peak near the walls of the CNNT in the figure - force the water molecules

to flow radially outwards in the cross-section of the nanotube by ~ 0.1 nm (almost one molecular diameter) more than when those rings are not present, such as for the pristine CNTs, which have a smoother potential energy landscape. This small molecular roughness induced by the triazine rings on the flow affects the local solid-liquid friction, and brings the local slip at the wall close to zero. The presence of three levels of flow roughness at the wall surface suggests the presence of a mixed slip system, with high slip near smooth graphitic patches on the surface, no-slip near the triazine rings (or any hydroxylated areas in the experiments), and somewhere in between near the C-N quaternary structures; the net effect is dominated by the lowest slip regions and their concentration over the entirety of the nanotube. In the case of CNNTs, the triazine rings and quaternary structures dominate the overall structure, leading to a drop in the overall slip length to below 1 nm. Figure 6b shows the MD results for radial velocity profiles in pristine CNT, turbostratic CNTs and CNNTs, indicating the calculated slip length, L_s, values for the three cases. The Hagen-Poiseuille flow Eq.(1) with MD-derived slip length is also shown, indicating reasonably good predictions for all cases.

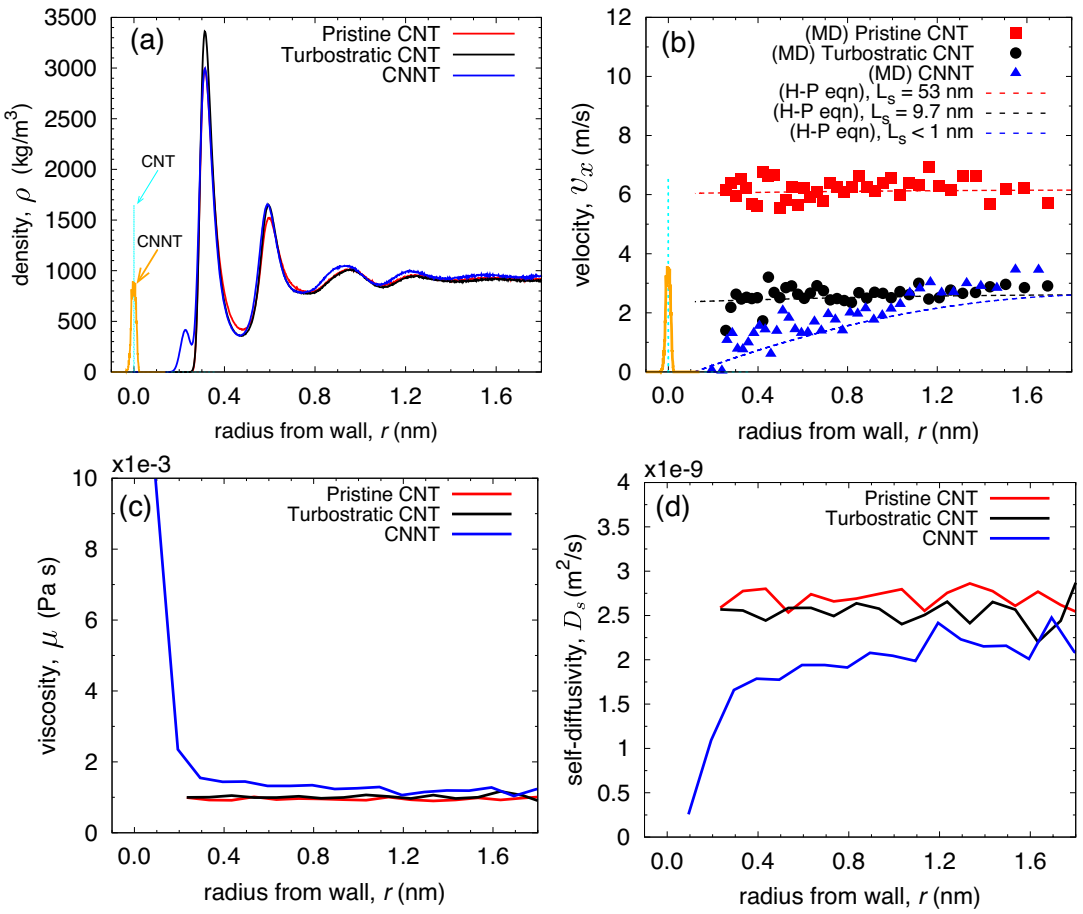

Figure 6. Radial profile measurements from the MD simulations of nanotube diameter $D = 4.071$ nm for (a) density, (b) velocity, (c) viscosity and (d) self-diffusivity, inside pristine CNTs (red), turbostratic CNTs, (black) and CNNTs (blue). In (a) oxygen atoms are only considered; similar results are obtained for the hydrogen atoms in the water molecule. In (b) comparisons are made with the Hagen-Poiseuille (H-P) flow Eq.(1) using dashed lines; applied pressure gradients in the MD are 1.15 ×

10^{14} Pa/m, 2.35×10^{14} Pa/m and, 1.32×10^{14} Pa/m for the pristine CNT, turbostratic CNT and CNNT, respectively.

A comparison of radial viscosity and self-diffusivity from the MD simulations also revealed an increased attraction of water near the surface of a CNNT, when compared to pristine and turbostratic CNTs, as shown in Figure 6c and Figure 6d, respectively. The water in the CNNT experiences an increased viscosity and a drop in self-diffusivity very close to the surface, whereas in the CNTs it retains the same values for viscosity and self-diffusivity near the surface as those in the bulk.[41] It is noted here that the measurements for bulk self-diffusivity are similar to those published for water on graphene in previous MD simulations (D_s = 2.6 x 10^{-9} m^2/s). This means that for CNNTs, the hydrophilisation caused by the nitrogen on the tube's surface, i.e. the increased surface/water potential energy (including the effect of partial charges) and also the increased levels of flow roughness near the surface, are causing the drop in transport of the water molecules near the surface.

Although the results clearly show that tube surface chemistry and structure do affect permeance, quantifying these effects is necessary to learn how to tailor the tubes' structure and chemistry for specific transport applications. The potential energy between the surface and the fluid is an obvious quantity to achieve this goal, as it can be directly obtained from the MD data. However, the challenge is that while CNTs have just one interatomic potential between solid and water, with CNNTs there are now two potentials (oxygen-carbon and oxygen-nitrogen) to consider, making it difficult to decouple the effect of each component. The authors have previously proposed a model to interpret the effect of solid-liquid interactions on flow which uses the concept of work of adhesion W_A, defined as the amount of work needed to detach the liquid from the solid and create two new interfaces. [42] This quantity allows measuring the overall attraction, inclusive of both surface structuring (i.e. physical roughness) and chemistry (i.e. energy roughness). The values for W_A, which have been obtained from the MD simulations in this work as a sum of potential energy over a unit area, are reported in Table 1. Values for pristine and turbostratic CNTs are in good agreement with experimental data previously reported,[7] giving further confidence about the value calculated here for CNNTs. Results in Table 1 clearly show an increase in the work of adhesion from pristine to turbostratic CNTs to CNNTs, in an inverse trend to contact angle. As $W_A = \pi_e + \gamma(1 + cos\theta)$,[42] this is not surprising. It should be noted, however, that the film pressure term, π_e, can be comparable in value to the surface tension for some materials including carbon,[42] and, hence, cannot be ignored.[7] Therefore, the work of adhesion can effectively link the properties of the tubes' wall to permeance of a fluid through it. This is a superior approach to using the contact angle for the same purpose as, in fact, there is no contact angle in a tube full of liquid (as the third and necessary phase – air – is missing). In Table 1, the values for the slip length, L_s, calculated from MD are also reported. Similarly to the work of adhesion values, those obtained for the pristine and turbostratic CNTs are in agreement with literature values of 98×10^{-3} and 144×10^{-3} J m^{-2}, respectively.[7, 17]

Table 1. Measured experimental and molecular dynamics data; Left: contact angles measured experimentally; Right: MD measurements for work of adhesion, slip length and the ratio of surface-diffusivity to work of adhesion.

Material	Contact angle (°)	reference	W_A (J m^{-2})	L_s (nm)	D_s/W_A (m^3 m^{-2} s^{-1} Pa^{-1})
Graphitic CNTs	82 - 86	[37]	105×10^{-3}	53	2.5×10^{-8}
Turbostratic CNTs	61 - 90	[15]	137×10^{-3}	9.7	1.9×10^{-8}
CNNTs	43 - 67	[this work]	175×10^{-3}	< 1	$(0.2\text{-}1.0) \times 10^{-8}$

By comparing the values for W_A and L_s, a similar inverse relationship is observed, with the more hydrophilic materials, i.e. those having the strongest interaction with water, resulting in the smallest slip length. All of these results point to a relationship between the nanotube wall physico-chemical material properties, the strength of the interaction between the tube wall and the liquid flowing through it, the hydrodynamics of the flow, i.e. the slip length, L_s, and the permeance, K. The authors have previously proposed on a model linking all of these properties,[7] which can be summarised in the two equations below:

$$\varepsilon = 1 + 8\frac{L_s}{D} = \frac{K_{exp}}{K_{HP}} \tag{4}$$

$$K_{exp} \approx \phi \frac{D_s}{W_A} \tag{5}$$

where K_{HP} is the no-slip permeance (derived from Eq.3 when L_s=0), K_{exp} is the permeance calculated from experimental data, and D_s is the surface diffusion arising from the chemical potential gradient present in pressure-driven flow. Eq.(5) is derived from first principles by replacing the Hagen-Poiseuille term and an expression linking L_s to D_s/W_A.[7] The last column in Table 1 reports the value for the D_s/W_A term obtained from MD data for the three materials investigated and Figure S 10 shows how Eq.(5) well compares with the experimental data for the CNNTs. A similar good agreement has already been shown with experimental data for turbostratic CNT membranes,[15] and with MD simulations of SiCNT and BNNT nanotubes.[17] Here, the approach of the model in Eq.(5) is further validated, representing a direct relation between permeance and solid-liquid interactions for a membrane of fixed porosity and nanotube material. This model can therefore be used to the design of aligned nanotube membranes that are tailored for specific applications, by controlling the transport of selected liquids using chemistry and structural changes inside the nanotubes.

Conclusion

Carbon nitride nanotubes were deposited in anodic alumina membranes using a non-catalytic synthesis method and the type of C-N bonds formed were characterized.

Pure water permeance measurements through CNNT membranes were compared to results obtained for CNTs in previous experimental work,[15] which similarly used an AAM support with uniform and parallel nanopores, and with MD simulations. The latter were conducted on nanotube models built as a faithful reproduction of the structure of the synthesised materials, using the information gathered by their characterisation and wettability. This approach goes beyond traditional MD simulations conducted on perfect nanotubes (e.g. pristine CNTs).

Both experiments and MD simulations showed that the presence of the C-N bonds hydrophilises the sp^2 carbon structure of the nanotubes, resulting in a decrease of the pure water permeance compared to pristine and turbostratic carbon nanotube membranes. These results are explained in terms of the strength of the solid-liquid interactions occurring at the tubes' walls, with the water at the CNNT walls showing increased water viscosity and decreased surface diffusion compared to CNTs. The combination of experiments and MD simulations presented here has allowed, for the first time, to decouple the effect of nanotube wall structure and surface chemistry on the flow of water through a nanotube membrane. The model and results presented in this paper offer membrane scientists a unique capability to design novel membranes and separation processes by way of controlling the permeance within nanotube membranes through membrane surface chemistry and structural changes to the nanotubes.

Methods

Synthesis of CNNTs membranes: The commercial symmetric AAMs used in this work were purchased from *Smartmembranes* and *Synkera* and had diameters ranging from 18 nm to 100 nm. Prior to CNNTs synthesis, all AAMs underwent a 1 hour annealing process at 30 ºC higher than the final synthesis temperature to increase their thermal resistance. The desired temperature was reached with a 1ºC/min ramp rate and the annealing was followed by natural cooling down.

CNNTs were deposited using non-catalytic chemical vapour deposition (CVD) in the pores of the AAMs using a melamine precursor (≥ 99% purity, purchased from *Sigma Aldrich*). The synthesis was carried out for 5 hours under a 200 sccm argon (Ar) flow in a quartz tube (ID 20 mm, OD 22 mm) heated up in the central section of a horizontal TZF 12/38/850 type CARBOLITE tubular furnace. Temperatures inside the furnace were monitored by external thermocouples. Gas flows were controlled with Omega FMAb5400A/5500A series mass flow controllers (MFCs) regulated by a LabVIEW program. Once the synthesis temperature of 520 ºC with a ramp rate of 10 ºC/min was reached, the melamine precursor was sublimated at 280 ºC in the first section of the tubular furnace. At completion of the synthesis, the system was left to cool naturally under Ar flow, and the sublimation of melamine was stopped by switching off the heating in the first section of the furnace. After synthesis, the CNNTs membranes were gently rinsed with deionised (DI) water.

The dissolution of the alumina templates of the CNNTs membranes was performed by reflux of H_3PO_4 (85 wt% in water, purchased from *Sigma Aldrich*) at 80ºC.

Synthesis of CNTs membranes: CNTs membranes used for the XPS analysis were prepared by CVD following the approach of Mattia et al.[15] The AAMs were pre-annealed at 900 ºC, which was reached with a ramp rate of 1 ºC/min. The membranes were then placed in the central zone of a tubular reactor, and heated to 670 ºC at 1 ºC/min in argon atmosphere. Once the maximum temperature was reached, the feed was switched to 3:7 ethylene:argon (120 sccm total) and was maintained in these conditions for 4 hours. After synthesis, the membranes were left to cool naturally under a gentle argon flow. The successful synthesis of the CNTs membranes lead to the synthesis of the nanotubes shown in Figure S 3.

Characterisation of CNNTs membranes: The produced membranes were fractured in small pieces, coated with 5 nm of chromium and positioned on carbon tape for analysis with a JEOL JSM-6301F FESEM. High magnification (> 90,000) FESEM images were taken with a Zeiss Sigma HD Field Emission Gun Analytical SEM (ASEM). The inner diameters of the tubes were calculated via statistical image analysis of FESEM micrographs using ImageJ by multiplying the obtained Feret's diameters by the circularity of the pores.[15]

JEOL JSM-2100Plus TEM samples were prepared following a similar procedure, finely grinding the membrane in an agate mortar prior to 1 hour and 20 minutes of dissolution in 1M NaOH. Each sample was then washed with vacuum filtration with a Nylon membrane (*Pall Corporation*) with 3 litres of water per AAM, suspended in 5 ml DI water and ultrasonicated in a VWR Ultrasonic Cleaner USC-T for 30 min. Two to five drops of the sample were then placed on a TEM window (Lacey carbon purchased from *EM Resolutions*) until a desirable concentration was reached. Analysis of structural features with ImageJ was done on a minimum of 10 measurements.

Contact angle measurements were obtained from sessile water droplets on carbon nitride deposited on alumina discs via the same synthesis method described for the deposition inside the AAMs. DI water was used as solvent for the sessile droplet method in air at 20 ºC with 2.5 µl droplets. Images of the drop were obtained using a Dataphysics Optical Contact Angle (OCA) Measuring Device each minute for 10 minutes per measurement. The accuracy of the machine is ± 2º. The Young contact angle (θ_Y) on a flat smooth surface is related to the measured contact angle (θ_W) using the Wenzel model:[43]

$$cos\theta_W = r\, cos\theta_Y, \tag{6}$$

where r is the ratio between the coated alumina disc surface area and the projected area, obtained by Atomic Force Microscope (AFM) Nanosurf easyScan 2 Flex.

Raman spectroscopy was performed on the as-produced CNNT membrane with UV light (wavelength 325 cm^{-1}) in a Renishaw InVia confocal Raman Microscope.

XPS was performed on powdered samples using a Thermo Fisher Scientific K-alpha+ spectrometer. Samples were analysed using a micro-focused monochromatic Al x-ray source (72 W) over an area of approximately 400 microns. Data was recorded at pass energies of 150 eV for survey scans and 40 eV for high resolution scan with 1 eV and 0.1 eV step sizes respectively. Charge neutralisation of the sample was achieved using a combination of both low energy electrons and argon ions. Data analysis was

performed in CasaXPS using a Shirley type background and Scofield cross sections, with an energy dependence of -0.6.

Permeation measurements: Pure water permeation tests took place in a horizontal dead-end filtration setup (as shown in the schematic in Figure 7 with 13 mm diameter stainless steel membrane holders with a 4 mm, 5 mm or 10 mm inner diameter effective area. The membrane holder was connected to a fluid flow measurement apparatus acquiring data via a Labview program. Pressure transducers P1 and P2 in Figure 7 (Swagelok industrial standard, 5kPa error) recorded the transmembrane pressure. A thermocouple (Omega, Type T) recorded the temperature. Ultrapure water (Veolia, 18.2 ΩM at 25 ºC) in a stainless steel syringe was driven by a pump (Nexus 6000) with a controllable flow rate. The rig was degassed with two valves positioned before and after the membrane holder (V1 and V2 in Figure 7). Each CNNT membrane was tested for at least one hour at stable transmembrane pressure. The water permeate was collected in a beaker pre-filled with a layer of silicone oil on a weighting scale (Mettler Toledo, MS304S/01, 0.1 mg sensitivity).

For each membrane, the permeance K was calculated as an average of four measurements at different syringe flow rates, employing the first equality introduced in Eq. (3).

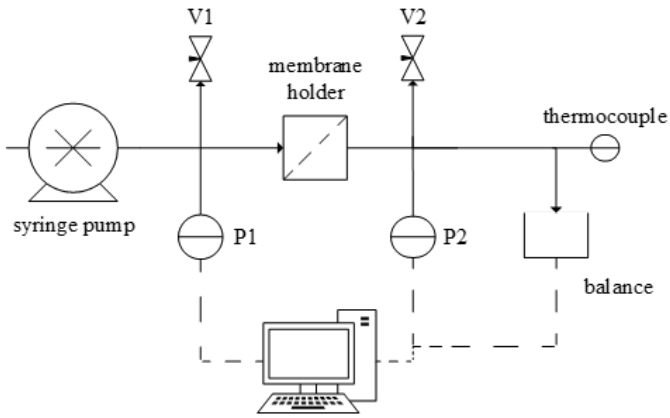

Figure 7. Schematic of the pressure-driven fluid flow measurement rig.

Computational Methodology: The LAMMPS platform[44] was used to perform high-fidelity molecular dynamics (MD) simulations of water flows through double-wall CNNTs. An example of an empty inner CNNT was given in Figure 3a, and a side view of a double-wall CNNT filled with water molecules is shown in Figure 8a. As a means of comparing MD flow results with previous experiments, we also simulate as benchmark cases flow through pristine double-wall CNTs (Figure 8b) and CNTs with 8.8% defects.

MD solves Newton's equations of motion for a system of molecules, which move deterministically in time and space, and interact together via potential energy functions; in this work we use the pair-wise Lennard-Jones (LJ) and electrostatic Coulombic potentials for all atoms in the flow simulations:

$$U_{ij} = 4\epsilon_{ij}\left[\left(\frac{\sigma_{ij}}{r_{ij}}\right)^{12} - \left(\frac{\sigma_{ij}}{r_{ij}}\right)^{6}\right] + \frac{1}{4\pi\epsilon_0}\frac{q_i q_j}{r_{ij}}, \quad (7)$$

where $\epsilon_{ij}$is the van der Waals interaction energy between a pair of interacting atoms (i, j), σ_{ij} is the characteristic length scale, r_{ij} is the distance between the atoms, q_i is

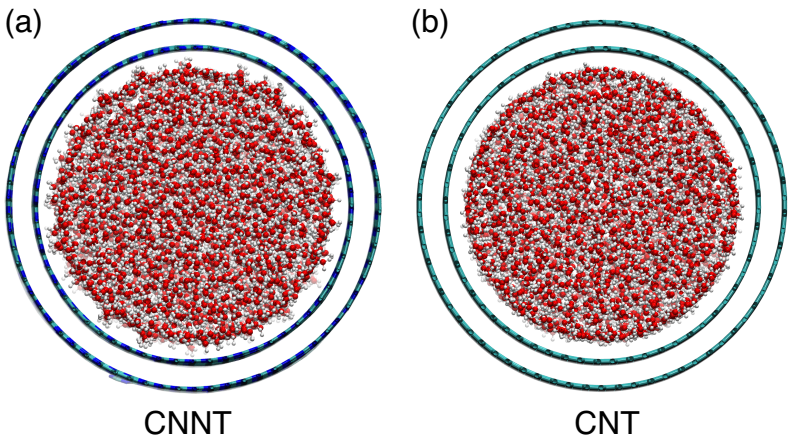

Figure 8. Cross-section of a MD simulation through (a) a CNNT and (b) a pristine CNT. The atoms are identified by the following colours: red = oxygen; white = hydrogen; cyan = carbon; blue = nitrogen.

the charge on one atom, and ϵ_0 is the vacuum permittivity.

The TIP4P/2005 model[45] along with the SHAKE algorithm is used for modelling water molecules, which consist of two hydrogen (H) atoms (0.5564 *e*), one LJ oxygen (O) atom and one massless (M) site (-1.1128 *e*). The PPPM method is used to evaluate all long-range Columbic interactions, while all short-range LJ interactions are shifted and truncated by a cut-off of 1.3 nm. An NVT MD ensemble is used in all flow cases, with an integration time-step of 2 fs.

In order to get the surface structure and chemistry in the MD simulation as close as possible to the experiment CNNTs, the surface was constructed with the same C:N (60:40) and pyridinic:quaternary (13:27 of N) ratios as the experiments. The CNNT is constructed by initially considering a CNT of known radius and chirality. Nitrogen atoms replace carbon atoms on the CNT in a spatially alternating pattern (i.e. quaternary sites initially occupying the full nanotube) that gives a ratio of 50:50 C:N. Pyridinic rings in various templates (sizes and orientations) are then generated, with number calculated from the above pyridinic:quaternary ratio, and are distributed randomly across the surface, avoiding overlap. The final step is then to bring down the amount of nitrogen atoms and quaternary sites by replacing nitrogen atoms with carbon atoms until 60% C is achieved in the nanotube; this process is performed randomly, and applied only in quaternary-dominated regions away from the pyridinic sites.

The wall atoms are equilibrated before being filled with water, using the reactive force field: ReaxFF,[46] which has the benefit of providing an equilibrated nanotube structure, and the unknown charges on all wall atoms using the charge equilibration technique.[47] In these pre-simulations, the total charge on the tubes was always zero. A timestep of 0.25 fs is only used for these LAMMPS pre-calculations. A sample of the

point charges on the CNNT surface was shown in Figure 3b. The wall atoms are then kept rigid for the water flow simulations that follow.

The remaining LJ potential parameters between the wall atoms and the water molecules were then obtained by calibration studies with our experiments. In the water-CNNT simulations, the oxygen-carbon potential parameters ϵ_{OC} = 0.102 Kcal/mol and σ_{OC} = 3.19 Å were already obtained from previous MD simulations[48] of water droplets on graphite surfaces, calibrated from an experimental contact angle of 86°,[49] and are used also for the CNNT in this work. We fix these oxygen-carbon parameters, and determine the missing nitrogen-oxygen parameters by calibrating a sessile nanodroplet using the experimental contact angle of 53° measured in this work. To do this, we construct a double-layered sheet of carbon-nitride, with similar structures as the CNNT and equilibrate a water droplet of 17.5k water molecules at 298 K on the surface as shown in Figure 9a. The size of the droplet was chosen large enough to be much bigger than the lengthscale of the biggest pyridinic structure on the surface, as well as to minimise line-tension effects. The length scale parameter for oxygen-nitrogen interaction was fixed and calculated from the Lorentz-Berthelot mixing rules, to be σ_{ON} = 3.234 Å. In each simulation, the oxygen-nitrogen energy parameter ϵ_{ON} is varied, and the equilibrium contact angle was measured as demonstrated in Figure 9b. From results in Figure 9 the energy parameter ϵ_{ON} = 0.1304 Kcal/mol is chosen to match the experimental 53° contact angle. These LJ parameters are then fixed for future flow simulations through the CNNTs.

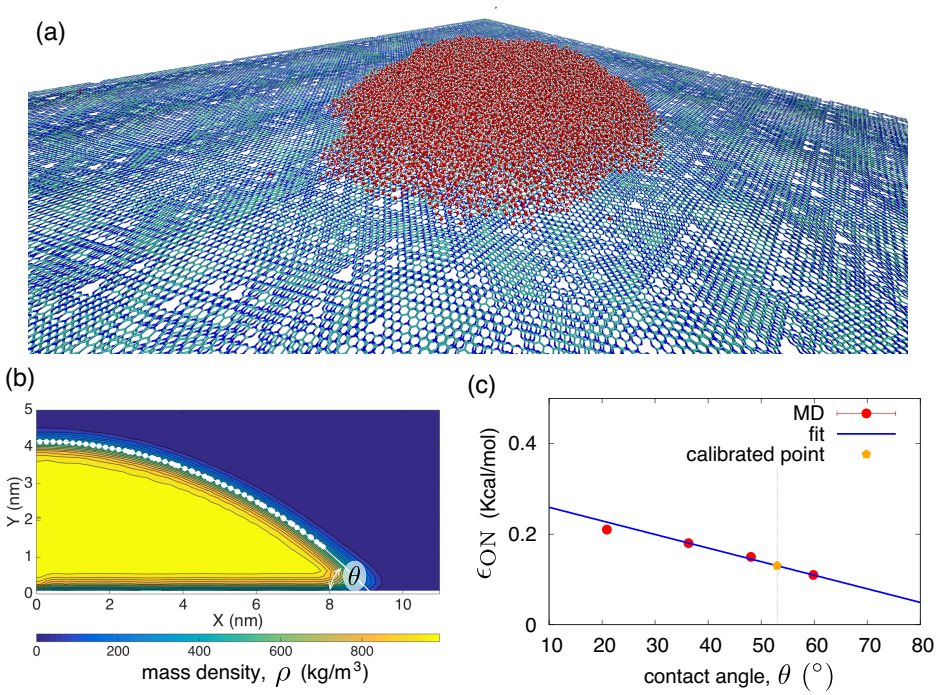

Figure 9. (a) MD case of a water droplet on a carbon nitride surface used for calibrating the Lennard-Jones energy parameter; (b) a density contour plot demonstrating how the contact angle is measured from the steady-state solution; (c) results of different MD simulations with varying ϵ_{ON}.

In the water-CNT simulations we use the same oxygen-carbon potential parameters as above, i.e. ϵ_{OC} = 0.102 Kcal/mol and σ_{OC} = 3.19 Å. For the turbostratic CNTs, however, we have modified the surface chemistry to contain ~8.8% point defects that matches the experiments, and recalibrated the oxygen-carbon potential parameters

using the same method as described above now with a target experimental contact angle of 61º, obtained as the lowest value from previous experimental data (see Table 1), [15] giving: ϵ_{OC} = 0.1162 Kcal/mol and σ_{OC} = 3.19 Å.

All nanotubes are filled with water at a target density of ~1000 kg/m^3, and allowed to equilibrate at 298 K using a Berendsen thermostat. The main simulation then consisted of applying a body force $F_x = \Delta p\ /\rho_n L$ (in the x-direction) to all water molecules, where ρ_n is the number density, and $\Delta p\ /L$ is the pressure gradient. The length of the nanotubes were all fixed at L = 15.74 nm. The steady-state average mass flow rate was measured using $\langle \dot{m} \rangle = m_i/L \sum_i v_{x,i}$ over ~10 ns of MD simulation time, where $v_{x,i}$ is the x-component velocity of a water molecule of mass m_i =2.99e-26 kg.

The nanotube flow resistance per unit length R was calculated using the linear flow relationship between pressure gradient and mass flow rate, i.e. $\Delta p/L = R\langle \dot{m} \rangle$, which is obtained by inspection of Eq.(1), and then used to calculate the slip length for a particular nanotube (geometry and surface chemistry) by rearranging Eq.(1) as follows:

$$L_s = \left(\frac{128\,\mu}{R\,\rho\pi D^4} - 1\right)\frac{D}{8}, \tag{8}$$

where D is the nanotube diameter, μ is the viscosity, and ρ is the mass density. The full-membrane permeance can be predicted by the theoretical model in Eq.(3), where all terms are known from the experiments, except the slip length L_s, which is calculated from the MD simulations, using Eq.(8). Note that Eq. (1) only includes Poiseuille pressure losses (i.e. due to the flow in the nanotube). However, entrance/exit pressure losses can be included in this equation[50-51] when the following constraint is true:[38]

$$L > \frac{3\pi D}{16\,\epsilon}\left(1 + \frac{8L_s}{D}\right), \tag{9}$$

where $\epsilon = 0.01$ is the error in the prediction. For example a typical experiment CNNT membrane carried out in this work has L_s < 1 nm, D = 80 nm and L = 50 μm; the RHS of Eq.(9) is ~5 μm. This means that CNNT membranes with nanotubes smaller than 5 μm require end losses to be incorporated in the flow prediction model of Eq. (1). As our membranes thicknesses (which correspond to L) are 10 times larger, we ignore end losses from our theoretical analysis.

The work of adhesion, viscosity and self-diffusion coefficient were obtained from equilibrium MD simulations of the D = 4 nm cases, but which contain no pressure-gradient forcing and so, no flow. The work of adhesion was computed by summing all potential energy interactions between wall and water molecules only, using Eq.(4), and then dividing over the wetted area of the nanotube ($\pi D\ L$). The viscosity, μ and the self-diffusion coefficient, D_s were then calculated using the Stokes-Einstein and Green-Kubo expressions, respectively,[26] in radial bins:

$$\mu = \frac{k_B T}{3\,\pi \alpha D_s}, \tag{10}$$

$$D_s = \frac{1}{N}\int_0^\infty \sum_{i=1}^{N} \langle v_{i,x}\,(t) \cdot v_{i,x}\,(t+t')\rangle\, dt', \tag{11}$$

where T is the fluid temperature, k_B is Boltzmann's constant, $\alpha = 1.7$ Å is the effective hydrodynamic diameter of one water molecule, N are the number of molecules in the bins and $v_{i,x}$ is the streamwise velocity of the i^{th} water molecule.

Acknowledgments

This research is supported by the Engineering and Physical Sciences Research Council (EPSRC), under grants EP/M01486X/1, EP/N016602/1, and EP/R007438/1. MKB thanks Sree Hari Perumanath and Nasser Afify from Edinburgh University for their useful discussions and MD support. SC thanks Dr. Jing Ji for her helpful remarks. The MD simulations were performed on ARCHER, the UK's national supercomputer. XPS data collection was performed at the EPSRC National Facility for XPS ('HarwellXPS'), operated by Cardiff University and UCL, under contract No. PR16195.

References

1. Majumder, M.; Chopra, N.; Andrews, R.; Hinds, B. J., Nanoscale hydrodynamics: Enhanced Flow in Carbon Nanotubes. *Nature* **2005,** *438* (7064), 44.

2. Whitby, M.; Quirke, N., Fluid Flow in Carbon Nanotubes and Nanopipes. *Nature Nanotechnology* **2007,** *2*, 87-94.

3. Mattia, D.; Gogotsi, Y., Review: static and dynamic behavior of liquids inside carbon nanotubes. *Microfluidics and Nanofluidics* **2008,** *5* (3), 289-305.

4. Das, R.; Ali, M. E.; Hamid, S. B. A.; Ramakrishna, S.; Chowdhury, Z. Z., Carbon nanotube membranes for water purification: A bright future in water desalination. *Desalination* **2014,** *336*, 97-109.

5. Song, X.; Wang, L.; Mao, L.; Wang, Z., Nanocomposite Membrane with Different Carbon Nanotubes Location for Nanofiltration and Forward Osmosis Applications. *ACS Sustainable Chemistry & Engineering* **2016,** *4* (6), 2990-2997.

6. Thomas, J. A.; McGaughey, A. J. H., Water Flow in Carbon Nanotubes: Transition to Subcontinuum Transport. *Physical Review Letters* **2009,** *102* (18), 184502.

7. Mattia, D.; Calabrò, F., Explaining high flow rate of water in carbon nanotubes via solid–liquid molecular interactions. *Microfluidics and Nanofluidics* **2012,** *13* (1), 125-130.

8. Secchi, E.; Marbach, S.; Niguès, A.; Stein, D.; Siria, A.; Bocquet, L., Massive radius-dependent flow slippage in carbon nanotubes. *Nature* **2016,** *537* (7619), 210-213.

9. Majumder, M.; Chopra, N.; Hinds, B. J., Effect of Tip Functionalization on Transport through Vertically Oriented Carbon Nanotube Membranes. *J. Am. Chem. Soc.* **2005,** *127* (25), 9062-9070.

10. Sinha, S.; Rossi, M. P.; Mattia, D.; Gogotsi, Y.; Bau, H. H., Induction and measurement of minute flow rates through nanopipes. *Physics of Fluids* **2007,** *19* (1), 013603-8.

11. Calabrò, F., Modeling the effects of material chemistry on water flow enhancement in nanotube membranes. *MRS Bulletin* **2017,** *42* (4), 289-293.

12. Khademi, M.; Sahimi, M., Molecular dynamics simulation of pressure-driven water flow in silicon-carbide nanotubes. *The Journal of Chemical Physics* **2011,** *135* (20), 204509-7.

13. Lin, X.; Yang, Q.; Ding, L.; Su, B., Ultrathin silica membranes with highly ordered and perpendicular nanochannels for precise and fast molecular separation. *ACS nano* **2015,** *9* (11), 11266-11277.

14. Lee, K. P.; Leese, H.; Mattia, D., Water flow enhancement in hydrophilic nanochannels. *Nanoscale* **2012,** *4* (8), 2621-2627.

15. Mattia, D.; Leese, H.; Lee, K. P., Carbon nanotube membranes: from flow enhancement to permeability. *Journal of Membrane Science* **2015,** *475*, 266-272.

16. Li, H.; Zeng, X. C., Wetting and interfacial properties of water nanodroplets in contact with graphene and monolayer boron–nitride sheets. *ACS nano* **2012,** *6* (3), 2401-2409.

17. Ritos, K.; Mattia, D.; Calabrò, F.; Reese, J. M., Flow enhancement in nanotubes of different materials and lengths. *Journal of Chemical Physics* **2014,** *140*.

18. Melillo, M.; Zhu, F.; Snyder, M. A.; Mittal, J., Water transport through nanotubes with varying interaction strength between tube wall and water. *The journal of physical chemistry letters* **2011,** *2* (23), 2978-2983.

19. Sendner, C.; Horinek, D.; Bocquet, L.; Netz, R. R., Interfacial water at hydrophobic and hydrophilic surfaces: Slip, viscosity, and diffusion. *Langmuir* **2009,** *25* (18), 10768-10781.

20. Ho, T. A.; Papavassiliou, D. V.; Lee, L. L.; Striolo, A., Liquid water can slip on a hydrophilic surface. *Proceedings of the National Academy of Sciences* **2011,** *108* (39), 16170-16175.

21. Bocquet, L.; Charlaix, E., Nanofluidics, from bulk to interfaces. *Chemical Society Reviews* **2010,** *39* (3), 1073-1095.

22. Joseph, S.; Aluru, N. R., Why Are Carbon Nanotubes Fast Transporters of Water? *Nano Letters* **2008,** *8* (2), 452-458.

23. Nicholls, W. D.; Borg, M. K.; Lockerby, D. A.; Reese, J. M., Water transport through carbon nanotubes with defects. *Molecular Simulation* **2012,** *38* (10), 781-785.

24. Walther, J. H.; Werder, T.; Jaffe, R. L.; Gonnet, P.; Bergdorf, M.; Zimmerli, U.; Koumoutsakos, P., Water-carbon interactions III: The influence of surface and fluid impurities. *Physical Chemistry Chemical Physics* **2004,** *6* (8), 1988-1995.

25. Corry, B., Water and ion transport through functionalised carbon nanotubes: implications for desalination technology. *Energy & Environmental Science* **2011,** *4* (3), 751-759.

26. Thomas, J. A.; McGaughey, A. J., Reassessing fast water transport through carbon nanotubes. *Nano letters* **2008,** *8* (9), 2788-2793.

27. Nicholls, W. D.; Borg, M. K.; Lockerby, D. A.; Reese, J. M., Water transport through (7, 7) carbon nanotubes of different lengths using molecular dynamics. *Microfluidics and nanofluidics* **2012,** *12* (1-4), 257-264.

28. Lu, X.; Wang, H.; Zhang, S.; Cui, D.; Wang, Q., Synthesis, characterization and electrocatalytic properties of carbon nitride nanotubes for methanol electrooxidation. *Solid State Sciences* **2009,** *11* (2), 428-432.

29. Miyamoto, Y.; Cohen, M. L.; Louie, S. G., Theoretical investigation of graphitic carbon nitride and possible tubule forms. *Solid state communications* **1997,** *102* (8), 605-608.

30. Wang, S.; Li, C.; Wang, T.; Zhang, P.; Li, A.; Gong, J., Controllable synthesis of nanotube-type graphitic C 3 N 4 and their visible-light photocatalytic and fluorescent properties. *Journal of Materials Chemistry A* **2014,** *2* (9), 2885-2890.

31. Bian, S.-W.; Ma, Z.; Song, W.-G., Preparation and characterization of carbon nitride nanotubes and their applications as catalyst supporter. *The Journal of Physical Chemistry C* **2009,** *113* (20), 8668-8672.

32. Wu, J.; Zheng, X.; Jin, C.; Tian, J.; Yang, R., Ternary doping of phosphorus, nitrogen, and sulfur into porous carbon for enhancing electrocatalytic oxygen reduction. *Carbon* **2015,** *92*, 327-338.

33. Liu, Q.; Duan, Y.; Zhao, Q.; Pan, F.; Zhang, B.; Zhang, J., Direct synthesis of nitrogen-doped carbon nanosheets with high surface area and excellent oxygen reduction performance. *Langmuir* **2014,** *30* (27), 8238-8245.

34. Ganesan, K.; Ghosh, S.; Krishna, N. G.; Ilango, S.; Kamruddin, M.; Tyagi, A., A comparative study on defect estimation using XPS and Raman spectroscopy in few layer nanographitic structures. *Physical Chemistry Chemical Physics* **2016,** *18* (32), 22160-22167.

35. Jorge, A. B.; Martin, D. J.; Dhanoa, M. T.; Rahman, A. S.; Makwana, N.; Tang, J.; Sella, A.; Corà, F.; Firth, S.; Darr, J. A., H2 and O2 evolution from water half-splitting reactions by graphitic carbon nitride materials. *The Journal of Physical Chemistry C* **2013,** *117* (14), 7178-7185.

36. Wang, Y.; Bayazit, M. K.; Moniz, S. J.; Ruan, Q.; Lau, C. C.; Martsinovich, N.; Tang, J., Linker-controlled polymeric photocatalyst for highly efficient hydrogen evolution from water. *Energy & Environmental Science* **2017,** *10* (7), 1643-1651.

37. Mattia, D.; Rossi, M. P.; Kim, B. M.; Korneva, G.; Bau, H. H.; Gogotsi, Y., Effect of Graphitization on the Wettability and Electrical Conductivity of CVD Carbon Nanotubes and Films. *Journal of Physical Chemistry B* **2006,** *110* (20), 9850 - 9855.

38. Weissberg, H. L., End correction for slow viscous flow through long tubes. *The Physics of Fluids* **1962,** *5* (9), 1033-1036.

39. Field, A., *Discovering statistics using IBM SPSS statistics*. sage: 2013.

40. Hummer, G.; Rasaiah, J. C.; Noworyta, J. P., Water conduction through the hydrophobic channel of a carbon nanotube. *Nature* **2001,** *414* (6860), 188.

41. Park, J. H.; Aluru, N., Ordering-induced fast diffusion of nanoscale water film on graphene. *The Journal of Physical Chemistry C* **2010,** *114* (6), 2595-2599.

42. Adamson, A. W.; Gast, A. P., *Physical Chemistry of Surfaces*. sixth ed.; Wiley-Interscience: New York, 1997.

43. Wenzel, R. N., Surface roughness and contact angle. *The Journal of Physical Chemistry* **1949,** *53* (9), 1466-1467.

44. Plimpton, S., Fast parallel algorithms for short-range molecular dynamics. *Journal of computational physics* **1995,** *117* (1), 1-19.

45. Abascal, J. L.; Vega, C., A general purpose model for the condensed phases of water: TIP4P/2005. *The Journal of chemical physics* **2005,** *123* (23), 234505.

46. Van Duin, A. C.; Dasgupta, S.; Lorant, F.; Goddard, W. A., ReaxFF: a reactive force field for hydrocarbons. *The Journal of Physical Chemistry A* **2001,** *105* (41), 9396-9409.

47. Rappe, A. K.; Goddard III, W. A., Charge equilibration for molecular dynamics simulations. *The Journal of Physical Chemistry* **1991,** *95* (8), 3358-3363.

48. Ritos, K.; Dongari, N.; Borg, M. K.; Zhang, Y.; Reese, J. M., Dynamics of nanoscale droplets on moving surfaces. *Langmuir* **2013,** *29* (23), 6936-6943.

49. Fowkes, F. M.; Harkins, W. D., The state of monolayers adsorbed at the interface solid—aqueous solution. *Journal of the American Chemical Society* **1940,** *62* (12), 3377-3386.

50. Ritos, K.; Borg, M. K.; Lockerby, D. A.; Emerson, D. R.; Reese, J. M., Hybrid molecular-continuum simulations of water flow through carbon nanotube membranes of realistic thickness. *Microfluidics and Nanofluidics* **2015,** *19* (5), 997-1010.

51. Borg, M. K.; Reese, J. M., Multiscale simulation of enhanced water flow in nanotubes. *MRS Bulletin* **2017,** *42* (4), 294-299.